LA-10126-PR
Progress Report

UC-33a
Issued: June 1984

LA--10126-PR

DE84 015074

Space Nuclear Safety Program

November 1983

Compiled by
S. E. Bronisz

Los Alamos National Laboratory
Los Alamos, New Mexico 87545

SPACE NUCLEAR SAFETY PROGRAM
November 1983

Compiled by
S. E. Bronisz

ABSTRACT

This technical monthly report covers studies related to the use of $^{238}PuO_2$ in radioisotope power systems carried out for the Office of Special Nuclear Projects of the US Department of Energy by Los Alamos National Laboratory. Most of the studies discussed here are ongoing. Results and conclusions described may change as the work continues.

I. GENERAL-PURPOSE HEAT SOURCE

A. Safety-Verification Impact Tests (D. Pavone and C. Frantz)

1. SVT-1. Metallographic examination of transverse cross sections of the individual cups of fueled clads HF-232 and HF-238 from the prime impact assembly of the first safety-verification module, SVT-1, indicated that the microstructures were uniform and generally fine grained, although the cup-to-cup variation was quite large, 20 to 28 grains per nominal 640-μm thickness (Table I).

Results of Auger electron spectroscopy (AES) analysis of the grain boundaries of these clads are listed in Table II. One sample of the HF-232 vent cup showed very low concentrations of thorium at both the interior and exterior edges and a moderately low level at the center of the specimen. Given the short aging time for the assembly (200 h), it is likely that the low thorium level does not represent depletion but that it indicates nonhomogeneous distribution. A shield-cup sample of HF-238 had small concentrations of sulfur and chlorine. This sample also had very high levels of carbon and oxygen, whereas the carbon and oxygen levels in the rest of the samples were low to moderate.

Principal impurity elements in the plutonia pellets are listed in Table III. With the exception of the calcium in pellet HF-410, all elements are well below the guide limits.

The quantity of plutonium released by the failed fueled clads was determined by radiochemical analysis of the ash resulting from combustion of the recovered graphite materials. The combustion ash of each sample was separated into size fractions >10 μm and <10 μm before dissolution for analysis. Details of the analysis are presented in Table IV. The total plutonium release was 110 mg; 12.8 mg was in the <10-μm fraction.

A sample of the >10-μm fraction from the ash of graphite impact shell (GIS) PGL-014 was examined under an electron microscope to determine if agglomeration of small particles (<10 μm) had occurred during the combustion process. Fig. 1 shows a micrograph of an agglomerated mass of small particles, individually less than 1 μm. This figure suggests that agglomeration does occur and that the analyzed results for the quantity of plutonium in particles <10 μm should be considered to be a minimum value.

2. SVT-2. The second safety-verification module, SVT-2, was subjected to a simulated minimum-gamma reentry thermal ramp and impacted flat-on at 54.19 ± 0.18 ms^{-1} and 917°C.

3. SVT-3. This test assembly was designated for testing at nominal orbital-decay reentry conditions. The components of the test assembly are identified in Table V. The impact assemblies were aged simultaneously in an ATJ (polycrystalline bulk) graphite furnace fixture at a clad temperature of 1287°C in a vacuum of less than 1 × 10^{-6} torr for 90 days. After a simulated reentry temperature pulse to 1375°C (clad), the module was impacted at 975°C (clad) and 54.4 ms^{-1}. During aging, three power interruptions occurred, two unplanned and

one planned. At 1391 h, a general power outage occurred; at 2027 h, the furnace was shut down to permit repair of the temperature recorder; and at 2069 h, a momentary interruption in cooling water flow occurred. In both unplanned shutdowns, the furnace protection devices functioned as designed to isolate the test object in the vacuum chamber. Aging was restarted with procedures identical to those used at the start of a test.

Helium release measurements indicated that there were several periods in which the release rate was equivalent to 75% of the generation rate (one vent plugged). These periods occurred in the initial 689 h of exposure.

The photographs in Fig. 2 illustrate the post-impact condition of the aeroshell. There were no cracks on either the impact face or the sides of the aeroshell, but a partial diagonal crack was present on the back side. Both GISs had longitudinal impact-face cracks and typical bowed profiles (Fig. 3).

The fueled clads (HF-343 and HF-350) in the prime impact assembly failed; only moderate localized deformation of the iridium was observed. A minor fracture occurred on the center of the back side of the HF-454 shield cup, but there were no failures of the iridium clad of HF-457. Photographs are shown in Fig. 4. Overall deformation of the fueled clads are listed in Table VI, along with the estimated area of the fracture. There was a significant quantity of vent effusate sur rounding the vent hole of HF-454.

The fracture patterns of the plutonia are shown in Fig 5. Pellets HF-343 and HF-350 were similar, consistin of radial, columnar fragments and nearly symmetrica overall deformation. The fracture pattern of HF-45 shows randomly oriented fragments, more nearly equi axed and generally larger than those of HF-343 o HF-350. The overall deformation is only slightly asym metric, and there appears to be no significant fue fragment displacement at the location of the failure i the shield cup. Radial, columnar fragments are als observed in HF-457, but the fragments are larger tha those in HF-343 and HF-350. Unsymmetric overal deformation, with a mild reverse bend in the clad at th impact face, can be seen.

The quantity of plutonium released during the impac was determined as for the SVT-1 test. Table IV sum marized the results.

Metallographic examination of a transverse cross sec tion through the fracture in the shield cup of HF-45 revealed a variable microstructure (Fig. 6). Large grains occupying 20-25% of the thickness, occurred on th interior of the shell throughout the section examined and at random locations on the exterior. The fracture mode was intergranular. A small reduction in thickness (about 4%) near the fracture indicated limited ductility.

Table I. Iridium Grain Size, GPHS SVT Series

Test No.	Clad No.	Cup No.	Diameter (μm)	Grains per 640 μm	Comments
SVT-1	FC-232	LR313-1(v)[a]	25.7	25	Uniform
	FC-232	LR316-1(s)	30.7	21	Uniform except for tab weld
	FC-238	LR315-2(v)	32.3	20	Uniform
	FC-238	LR318-6(s)	23.3	28	Uniform
	FC-261	P709-6(v)	29.1	22	Uniform
	FC-261	Q804-1(s)	29.8	22	Uniform
	FC-410	S2-5(s)	31.6	20	Uniform
SVT-3	FC-343	PR718-5(v)	32.7	20	Lg. int. grains, 20-25% of thk.
	FC-343	PR719-5(s)	38.9	16	Lg. int. grains, 20-25% of thk.
	FC-350	R904-7(v)	35.7	18	Lg. int. grains, 20-25% of thk.
	FC-350	R904-5(s)	36.4	18	Lg. int. grains, 20-25% of thk. and tab weld
	FC-454	S39-5(s)	42.3	15	Lg. int. grains, 20-25% of thk. + isolated lg. ext. grains

[a](v) — vent cup; (s) — shield cup.

TABLE II. Results of Auger Electron Spectroscopy Analysis of Prime Iridium Clads from SVT-1

Specimen	Location	$\frac{Th_{65}}{Ir_{229}}$	$\frac{C_{270}}{Ir_{229}}$	$\frac{O_{510}}{Ir_{229}}$	Other
FC-232	Int. edge	0.07	0.45	0.48	
Vent cup-1	Center	0.40	0.33	0.79	
	Ext. edge	0.16	0.62	0.68	
	Average	0.21	0.47	0.65	
VC-232	Int. edge	0.46	0.28	0.60	
Vent cup-2	Center	0.56	0.28	0.85	
	Ext. edge	0.61	0.49	0.82	
	Average	0.54	0.35	0.76	
FC-232	Int. edge	0.36	0.14	0.36	
Shield cup-1	Center	0.65	0.13	0.38	
	Ext. edge	0.57	0.23	0.55	
	Average	0.53	0.17	0.43	
FC-232	Int. edge	0.71	0.16	0.27	
Shield cup-2	Center	0.75	nd[a]	nd	
	Ext. edge	0.60	0.19	0.34	
	Average	0.69	0.12	0.20	
FC-238	Int. edge	0.45	0.35	0.69	
Vent cup-1	Center	0.76	0.21	0.43	
	Ext. edge	0.44	0.75	0.93	
	Average	0.55	0.44	0.69	
FC-238	Int. edge	0.55	0.27	0.77	
Vent cup-2	Center	0.65	0.22	0.44	
	Ext. edge	0.41	0.40	0.55	
	Average	0.56	0.30	0.59	
FC-238	Int. edge	0.41	1.75	0.99	S-0.05, Cl-0.12
Shield cup-1	Center	0.50	1.55	1.40	S-0.03
	Ext. edge	0.43	1.06	1.12	S-0.05
	Average	0.45	1.45	1.17	S-0.04, Cl-0.04
FC-238	Int. edge	0.80	0.19	nd	
Shield cup-2	Center	0.88	0.15	nd	
	Ext. edge	0.80	0.17	nd	
	Average	0.83	0.17	nd	

[a]nd—not detected.

TABLE III. Plutonia Analysis, GPHS SVT Series

Test No.	Pellet No.	Selected Elements (ppm)								
		P[a]	Mg	Ca	Al	Si	Fe	Cr	Ni	Ti
SVT-1	HF-232	5	1	130	20	15	60	15	nd[b]	5
	HF-238	5	1	200	25	70	70	15	5	5
	HF-261	5	nd	200	20	25	85	40	nd	7
	HF-410	2	3	400	25	45	110	35	5	7
SVT-2	HF-350	3	nd	200	35	20	35	10	nd	20
	HF-343	5	10	100	35	30	20	10	nd	15
	HF-454	2	nd	200	60	50	70	60	nd	20
	HF-457	3	nd	150	35	10	20	15	nd	3

[a]Colorimetric analysis.
[b]nd—not detected.

TABLE IV. Fuel Release from SVT Modules

Test No.	Component	Pu Content (g)		
		<10 μm	>10 μm	Total
SVT-1	Impact shell, intact clads	0.0010	0.0034	0.0044
	Impact shell, failed clads	0.0074	0.0710	0.0784
	Aeroshell and insulation	0.0039	0.0196	0.0235
	Catch-tube debris	0.0005	0.0032	0.0037
	Total	0.0128	0.1072	0.1100
SVT-3	Impact shell, intact clads	0.0006	0.0004	0.0010
	Impact shell, failed clads and aeroshell	0.0018[a]	0.0090	0.0108
	Catch-tube debris	0.0027	0.0032	0.0059
	Total	0.0051	0.0126	0.0177

[a]Estimated.

TABLE V. SVT-3 Test Assembly Components

Component	Serial No.
Aeroshell	PAL-014
Prime impact assembly	
Impact shell	PGL-020
Fueled clads	FC-343, FC-350
Fuel pellets	HF-343, HF-343
Insulation sleeve	C40-7
Insulation disks	P8-2-59, P8-2-60
Secondary impact assembly	
Impact shell	PGL-027
Fueled clads	FC-454, FC-457
Fuel pellets	HF-454, HF-457
Insulation sleeve	C30-4
Insulation disks	P11-1-24, P11-1-31

TABLE VI. Impact Test Summary, GPHS SVT Series

			Gross Deformation			Failures	
Test No.	Reentry Mode	Fueled Clads	Diam (%)	Height (%)	Axial (%)	Number	Total Area (mm^2)
SVT-1	Min-γ[a]	FC-232(P)[b]	+13.5	−11.1	+5.8	0	
		FC-238(P)	+9.6	−7.3	+3.8	0	25.4
	Face-on	FC-261(S)	+11.7	−11.1	+5.6	2	
		FC-410(S)	+9.8	−9.6	+1.4	1	
SVT-3	Orbital	FC-343(P)	+12.3	−9.0	+5.7	0	
	decay[c]	FC-350(P)	+10.0	−8.5	+2.6	0	0.4
	Face-on	FC-457(S)	+10.8	−7.2	+5.6	0	
		FC-454(S)	+9.5	−6.4	+2.9	1	

[a] Aged 200 h at 1287°C (clad). Impact 919°C and 54 ms^{-1}.
[b] (P)—prime; (S)—secondary.
[c] Aged 90 days at 1287°C (clad). Impact 975°C and 54 ms^{-1}.

Typical microstructures of transverse sections of the iridium cups of the prime fueled clads HF-343 and HF-350 are shown in Fig. 7. All four samples had nonuniform microstructures, with large grains on the interior. Typically, 20-25% of the thickness consisted of one or two grains. The average grain sizes are listed in Table I. The shield cup of HF-343 had a larger grain size than the other iridium cups in SVT-3, but all are considerably finer grained than the seven to eight grains across the wall predicted from previous observations.

A region of the shield-cup cross section of HF-350 exhibiting a columnar microstructure with some grains showing a substructure similar to that seen in weld metal is shown in Fig. 8. This structure is similar to that observed at the fracture site of the shield cup of HF-261 in the SVT-1 test. The appearance of the weld metal substructure and the columnar grains normal to the thickness direction of the clad wall identify this region as that of the laser weld used to attach the weld shield tab. This microstructure is not characteristic of a large fraction of the cup, but is a structure susceptible to cracking if subjected to bending with the tensile stress on the interior.

The weld cross sections of both prime fueled clads indicated full penetration welds with no porosity and desirable microstructures. Metallographic cross sections are shown in Fig. 9.

Because of the appearance of vent effusate on HF-454, the vent assembly of this secondary fueled clad was sectioned and examined. There were nonmetallic deposits in the filter element (principally at the entrance to the vent assembly), porous vapor-transported iridium-tungsten alloy on the wall of the vent orifice (Fig. 10), and intermetallic reaction products on the exterior of the clad surrounding the vent orifice, as shown in Fig. 11. Electron microprobe analysis indicated the phases at the vent entrance contained iron, silicon, calcium, plutonium, titanium, tungsten, manganese, and oxygen. Deposits at the interior of the vent orifice consisted of phases containing silicon, aluminum, and oxygen; calcium, silicon, and oxygen; silicon, calcium, titanium, iron, aluminum, magnesium, and oxygen; and plutonium, silicon, calcium, titanium, aluminum, chromium, iron, and oxygen. Four phases, identified in the intermetallic reaction product on the exterior of the clad, consisted of (a) iridium, tungsten, and iron; (b) iridium, plutonium, and titanium; (c) iridium and plutonium; and (d) iridium and iron. Although the vent-assembly and decontamination-cover welds were sound, extremely large grains were present in the welds.

Results of AES analysis of the grain-boundary chemistry of the iridium of the prime fueled clads and the shield cup of HF-454 are presented in Table VII. The results indicate some depletion of the thorium concentration of the interior edge in all samples. The overall thorium level appears to be somewhat low relative to that generally observed in DOP-26 iridium alloy. Carbon and oxygen occur in widely varying amounts. The most significant observation is the presence of sulfur in large amounts in both samples from the shield cup of HF-454. The samples were taken to include metal adjacent to the fracture. Although there is considerable difference in the sulfur concentrations in the two samples, their location near the fracture indicates that the sulfur contamination probably was the principal cause of the failure.

Table III contains the analyses of selected impurity elements in the plutonia pellets. The phosphorus was determined colorimetrically and the rest by emission spectrography. The samples analyzed indicate that the levels of all elements except calcium were below the impurity guideline limits. Phosphorus in all four pellets is very low, among the lowest observed since phosphorus analyses were included in post-mortem examinations.

The quantity of plutonium released from the fueled clads was determined by procedures previously described in the post-mortem of test SVT-1. Table IV gives the details. The <10-μm sample of the ash from GIS PGL-020, the aeroshell, and large pieces of insulation were lost because of failure of the sealed quartz tube during the dissolution operation. An estimated value for this analysis is given in the table. The total plutonium released was 17.7 mg, with 5.1 mg in the <10-μm range.

4. SVT-4. The aging exposure of this test assembly was completed on November 23, 1983. The exposure time was 2164 h. Three unscheduled furnace shutdowns occurred during the exposure. At 606 h, a general power outage occurred and, at 733 h, the furnace shut down because of failure of the electric motor on the mechanical pump of the leak detector. After this second shutdown, the test pieces were removed from the furnace, transferred to the inert-atmosphere glove box and inspected. No abnormalities were observed, and the exposure was continued after the equipment was repaired and satisfactory operation of the vacuum system was demonstrated. The test pieces were stored in the inert-atmosphere glove box (O_2 < 150 ppm) for 4 days, and the aging was resumed according to standard start-up procedures. At 1279 h, a momentary interruption of cooling water flow to the laboratory caused a third shutdown. All protection devices operated as designed, and the aging was resumed the following day.

After the aging was completed, SVT-4 was subjected to a simulated orbital-decay reentry thermal ramp and impacted flat-on at 54 ms^{-1} and 975°C.

TABLE VII. Results of Auger Electron Spectroscopy Analysis of Iridium Clads from SVT-3

Specimen	Location	Th_{65} / Ir_{229}	C_{270} / Ir_{229}	O_{510} / Ir_{229}	S_{150} / Ir_{229}
HF-343	Int. edge	0.38	0.19	0.55	nd[a]
Vent cup-1	Center	0.68	nd	nd	nd
	Ext. edge	0.41	0.50	0.77	nd
	Average	0.49	0.23	0.46	nd
HF-343	Int. edge	0.17	0.47	0.57	nd
Vent cup-2	Center	0.48	0.39	0.73	nd
	Ext. edge	0.39	0.58	0.80	nd
	Average	0.35	0.48	0.70	nd
HF-343	Int. edge	0.21	0.41	0.85	nd
Shield cup-1	Center	0.35	0.29	0.80	nd
	Ext. edge	0.41	0.29	0.91	nd
	Average	0.32	0.33	0.85	nd
HF-343	Int. edge	0.35	nd	0.34	nd
Shield cup-2	Center	0.76	nd	0.33	nd
	Ext. edge	0.55	nd	0.37	0.02
	Average	0.55	nd	0.35	0.01
HF-350	Int. edge	0.19	0.95	0.59	nd
Vent cup-1	Center	0.63	0.65	0.73	nd
	Ext. edge	0.47	1.02	0.79	nd
	Average	0.43	0.87	0.70	nd
HF-350	Int. edge	0.46	nd	nd	nd
Vent cup-2	Center	0.74	nd	nd	?
	Ext. edge	0.84	nd	nd	nd
	Average	0.68	nd	nd	nd
HF-350	Int. edge	0.20	1.85	0.94	0.03
Shield cup-1	Center	0.44	1.33	1.15	nd
	Ext. edge	0.41	1.44	0.80	nd
	Average	0.35	1.54	0.96	0.01
HF-350	Int. edge	0.14	nd	nd	nd
Shield cup-2	Center	0.75	nd	nd	nd
	Ext. edge	0.65	0.17	0.26	nd
	Average	0.51	0.06	0.09	nd
HF-454	Int. edge	0.32	0.99	0.59	0.11
Shield cup-1	Center	0.48	0.83	0.96	0.14
	Ext. edge	0.59	1.12	0.87	0.19
	Average	0.46	0.98	0.81	0.15
HF-454	Int. edge	0.16	0.77	0.78	vs[b]
Shield cup-2	Center	0.28	0.56	1.12	vs
	Ext. edge	0.36	0.84	0.95	vs
	Average	0.24	0.72	0.95	vs

[a] nd—not detected.
[b] vs—very strong.

5. SVT-5. As of December 1, 1983, the accumulated exposure time of the fifth safety-verification module was 1955 h. No evidence of vent plugging has been detected by the continuous helium-release measurements.

B. Explosion Test (R. Tate)

The iridium fragments recovered after the DIRECT COURSE explosion are shown in Fig. 12. None of them were found by visual searching; all were detected because of the gamma activity that was induced by neutron irradiation before the test.

C. Fragment Test (R. Tate)

The second and third engineering development runs for the GPHS fuel-tank fragment test were conducted at Sandia National Laboratories' 1.5-km rocket sled track. The objective of these runs was to develop a catch-box system to recover the target objects, the iridium clads, in the actual GPHS module test. The targets again were Styrofoam blocks with four steel slugs simulating the GPHS fuel capsules. The aluminum plate fragment was released closer to the target than in the first development run.

The catch box in the second run was a long box fabricated from 6-mm steel plate, lined with 18-mm plywood, and filled with vermiculite. The catch-box dimensions were 4.6 m long with a 25- by 25-cm cross section. In this second run, the end of the catch box was 43 cm from the target to allow room for the furnace shell that will be used in the actual test to heat the module stack. The catch box was suspended from an A-frame by a pair of 3-mm steel cables. After the second run, the four steel slugs were found on the ground between the target and the mouth of the catch box.

For the third development run, the experimental setup was similar but the box was supported by four cables. The suspension was articulated so that the catch box could be withdrawn to clear the furnace shell during the pre-impact heating phase. At −15 s, the catch box was released by a winch so that the box opening was 25 mm from the target. After this third run, the two trailing steel slugs were found in the catch box.

D. Leaking Fueled Clads (J. Archuleta)

Several early-production fueled clads for the GPHS were found to have leaky vent assemblies during decontamination at the Mound Facility. Two such fueled clads, HF-104 and HF-219, were sent to Los Alamos for examination.

The vent end was removed from each capsule, and the fuel was returned to the Savannah River Plant for reprocessing; the remaining iridium was stored for future disposition. The vents were examined and photographed with an optical microscope and with the scanning electron microscope (SEM). They were then sectioned diametrally and the exposed surfaces were prepared metallographically, examined, and photographed.

The external surfaces of the vent assemblies are shown in Fig. 13. A crack at the inner edge of the decontamination-cover weld of HF-104 is visible at 10 o'clock (Fig. 13a). A similar crack is barely visible in the same region of HF-219 (Fig. 13b). The reverse sides of the vents appeared normal (Figs. 13c and 13d).

At higher magnification and with the greater depth of field inherent in the SEM, the cracks were clearly visible on the inner circumference of the decontamination-cover weld (Fig. 14). About 20% of the circumference was cracked on HF-104, and about 15% was cracked on HF-219.

After the SEM examination, the vents were sectioned diametrally through the cracks and prepared metallographically. These sections confirmed that the cracks breached the decontamination covers of both vents (Fig. 15) and were the cause of the leaks. Barely visible in HF-104 is a nonbreaching weld crack opposed to the breach. At higher magnification (Fig. 16), we see that each of the cracks occurred in the same relative region, slightly away from the fillet of the weld.

As expected, etching revealed that the cracks were intergranular (Fig. 17). They occurred in the columnar grains that resulted from the directional solidification of the weld-fused metal.

Neither decontamination cover showed external damage, and both were displaced outward suggesting that internal pressure caused the failures.

Although the exact internal pressure cannot be calculated without a detailed knowledge of the temperature history of the fueled clads from the time of the final closure of the assembly weld, it seems unlikely that a pressure differential of much more than 1 atm could have been reached. An internal differential pressure of 1 atm would produce a radial stress at the crack location of 138 MPa (20 000 psi), well below the yield stress of normal polycrystalline iridium. The columnar weld grains cause a local departure from polycrystallinity that results in a straight grain-boundary path through the decontamination cover. Any source of additional stress, such as the residual stress in the decontamination cover, together with the inherent stress raiser at the surface-tension groove where the grain boundary intersects the surface could lead to the start of the crack.

II. ENVIRONMENTAL SUPPORT (C. Land)

Four 37-g $^{238}PuO_2$ pellets, a 46.5-g pellet, and a large fragment of a pellet that had been exposed to aqueous environments for extended periods were sectioned, prepared ceramographically, and examined. The only evidence of interaction between the pellets and their environments was an enhanced reaction of the exposed surfaces to the etchant used to delineate the grain boundaries.

A. Seawater

Pellet ET 2-6 was immersed in simulated seawater for 943 days at 35°C. We saw no evidence of erosion or corrosion of the pellet in the as-polished condition (Fig. 18), but the highly porous areas at the end and circumference of the pellet (Fig. 19) were attacked preferentially by the etchant (Fig. 20) to a depth of ~300 μm. This effect was not observed along a freshly broken edge (Fig. 21) where the density was greater.

Pellet ET 1-5 was immersed in simulated seawater for 943 days at 10°C. There was no evidence of reaction between the seawater and the pellet in the as-polished condition (Fig. 22), but etched, the surface exposed to the seawater was ragged (Fig. 23). The depth of damage was <50 μm. The porosity along the edge was less than that in the 35°C seawater test pellet (Fig. 24).

A 32.4-g piece from $^{238}PuO_2$ pellet HPZ-186-2 was held in simulated seawater for 682 days at 10°C. There was no apparent damage to the exposed surfaces (Figs. 25 and 26).

A 46.5-g $^{238}PuO_2$ pellet, HPZ-174-2, was immersed in simulated seawater for 1855 days at 10°C. There was no major damage to the exposed surface, but a little material was removed from near the surface during etching (Figs. 27 and 28).

B. Fresh Water

Pellet ET 2-4 was immersed in fresh water for 943 days at 35°C. There was a high density band along the end of the pellet and a low density band along the side, as shown in Fig. 29. There was no evidence of a reaction having occurred along the side of the pellet when it was in the as-polished condition (Fig. 30), but etched, the surface showed void enhancement along the edge (Fig. 31).

Pellet ET 2-2 was immersed in fresh water for 943 days at 10°C. There was no evidence of a reaction having taken place along the exposed side of the pellet in the as-polished condition (Fig. 32), but the etched exposed edge was ragged (Fig. 33).

III. SAFETY TECHNOLOGY (D. Peterson)

Several phenomena observed in $^{238}PuO_2$ heat sources have not been explained, such as anomalous iridium grain growth, disappearance of thorium from the iridium grain boundaries, vapor transport of plutonium and fuel impurities, pitting on iridium grain boundaries, and phosphorus retention in the fuel. Analyzing the interactions of the heat source components is difficult because of the unknown phases that could form given the appropriate conditions. Compounds that could be important to this analysis include $PuPO_4$, PuP_2O_7, $Ca(PO_3)_2$, $Ca_2P_2O_7$, $Ca_2Pu(P_2O_7)_2$, $ThIr_3C_x$, $ThIr_3P_x$, $PuIr_2C_x$, and $PuIr_2P_x$. (Only the first four phases are known to exist.)

This month $PuPO_4$ was prepared by heating a mixture of PuO_2 and excess P_2O_5 at 1000°C for 4 h in flowing air. The sample transformed from green-brown to bright blue. The composition was identified by x-ray diffraction as predominately $PuPO_4$ with a small amount (5%) of PuP_2O_7. When the $PuPO_4$ was heated in a platinum crucible to 1300°C for 1 h, the platinum reacted with it and became very brittle.

$PuPO_4$, P_2O_5, and CaO were heated in an alumina cell to 1000°C for 1 h in flowing air in an attempt to form $Ca_2Pu(P_2O_7)_2$. The components reacted, melted, and formed a bright purple compound, which has been submitted for x-ray diffraction analysis. The fact that the reaction product had a melting point below 1000°C gives us some hope that this or another compound will lead us to an explanation of the impurity transport and vent-plugging phenomena.

IV. FIVE-WATT HEAT SOURCE (D. Pavone)

The heat source of the 5-W radioisotopic thermoelectric generator (RTG) consists of two 62.5-W(t) GPHS fueled clads in a GIS. This impact assembly, contained in a bulk graphite housing, was impacted at 13.4 ms^{-1} and an iridium clad temperature of 501°C. The orientation of the impact was end-on on the nonclosure end of the impact shell.

No significant damage to the GIS occurred and only minor deformation of the fueled clads was visible, principally on the impact end of the lead fueled clad, HF-421. Fig. 34 shows a photograph of the impacted test assembly and Fig. 35 shows the fueled clads. Dimensions of the fueled clads are tabulated in Table VIII.

A photomacrograph of an axial cross section of the end of the shield cup of the lead fueled clad, HF-421, is shown in Fig. 36a. This section illustrates minimal deformation sustained by the iridium. Fig. 36b shows an as-polished photomicrograph of the impact end of the cladding and reveals several small cracks on the interior surface. In general, the cracks are limited to a depth of one grain, as shown in Fig. 36c.

TABLE VIII. Dimensions of the Fueled Clads of the 5-W RTG Heat Source

	Av Diam (in.)		Axial Length
Clad No.	Vent Cup	Shield Cup	(in.)
FC-421			
Pre-Impact	1.175	1.174	1.186
Post-Impact	1.177	1.177	1.193
FC-420			
Pre-Impact	1.175	1.177	1.187
Post-Impact	1.176	1.180	1.193

Fig. 1. Agglomerated particles in the >10-μm fraction of the combustion ash of GIS PGL-014 of SVT-1 (10 000X).

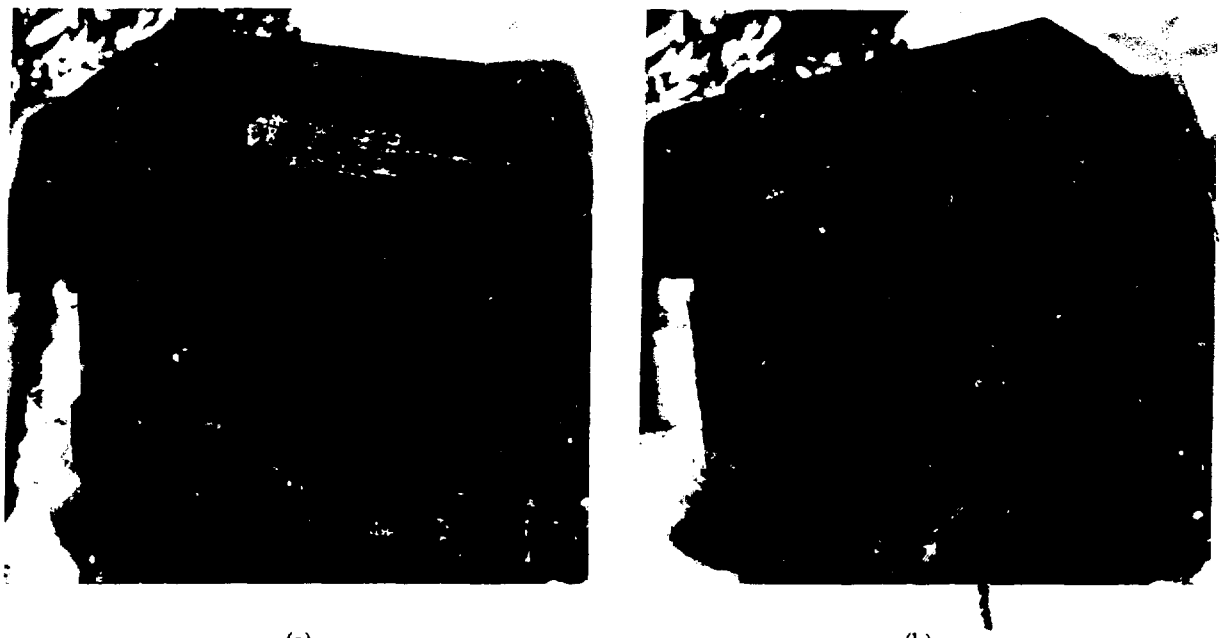

(a) (b)

Fig. 2. Impacted test assembly SVT-3: (a) no fractures on the impact face or sides of the aeroshell; (b) a partial diagonal crack on the back side (0.6X).

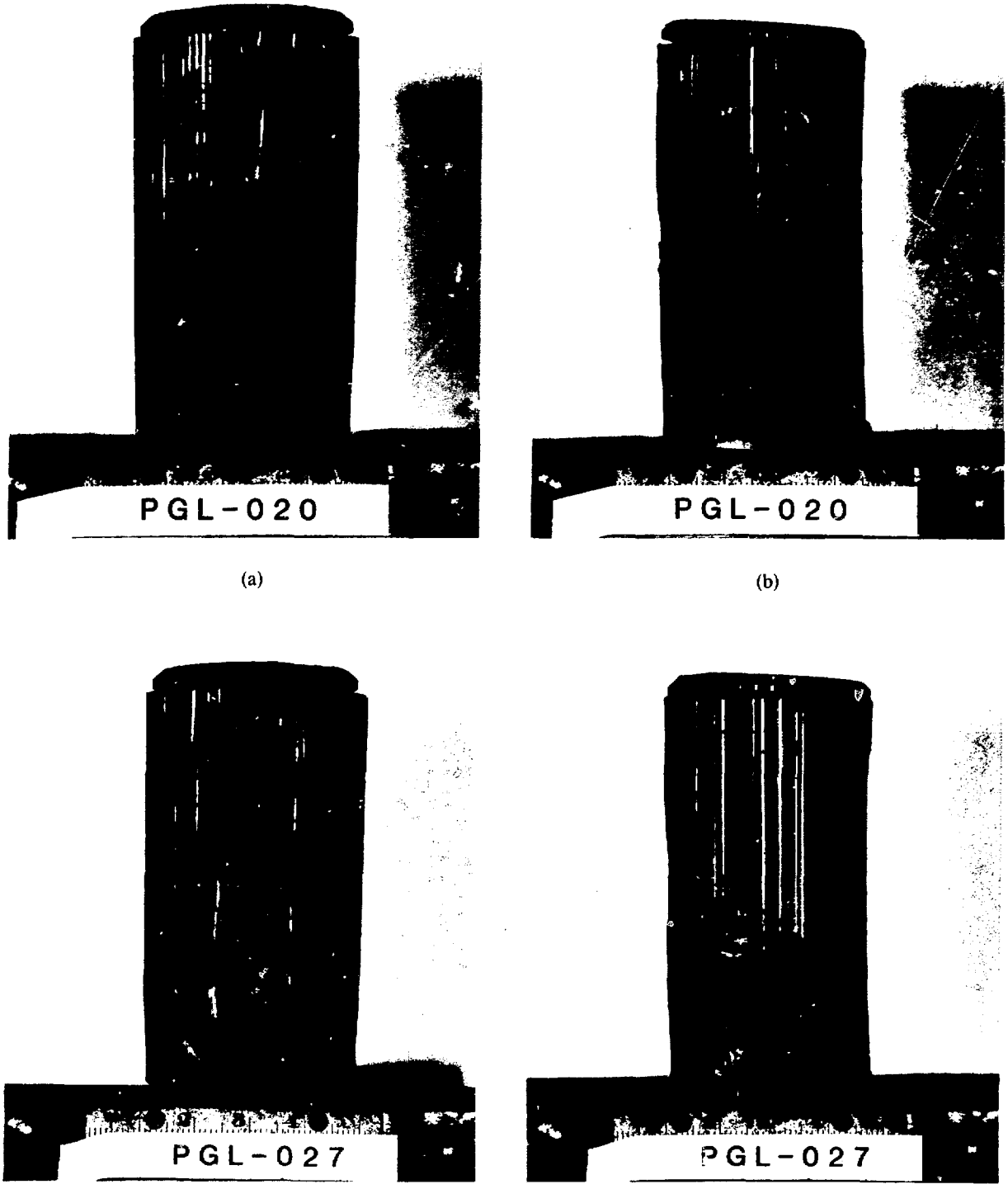

Fig. 3. Graphite impact shells from test SVT-3 showed longitudinal cracks on the impact face and bowed profiles after the test: (a) PGL-020 impact face; (b) PGL-020 side; (c) PGL-027 impact face; (d) PGL-027 side (0.95X).

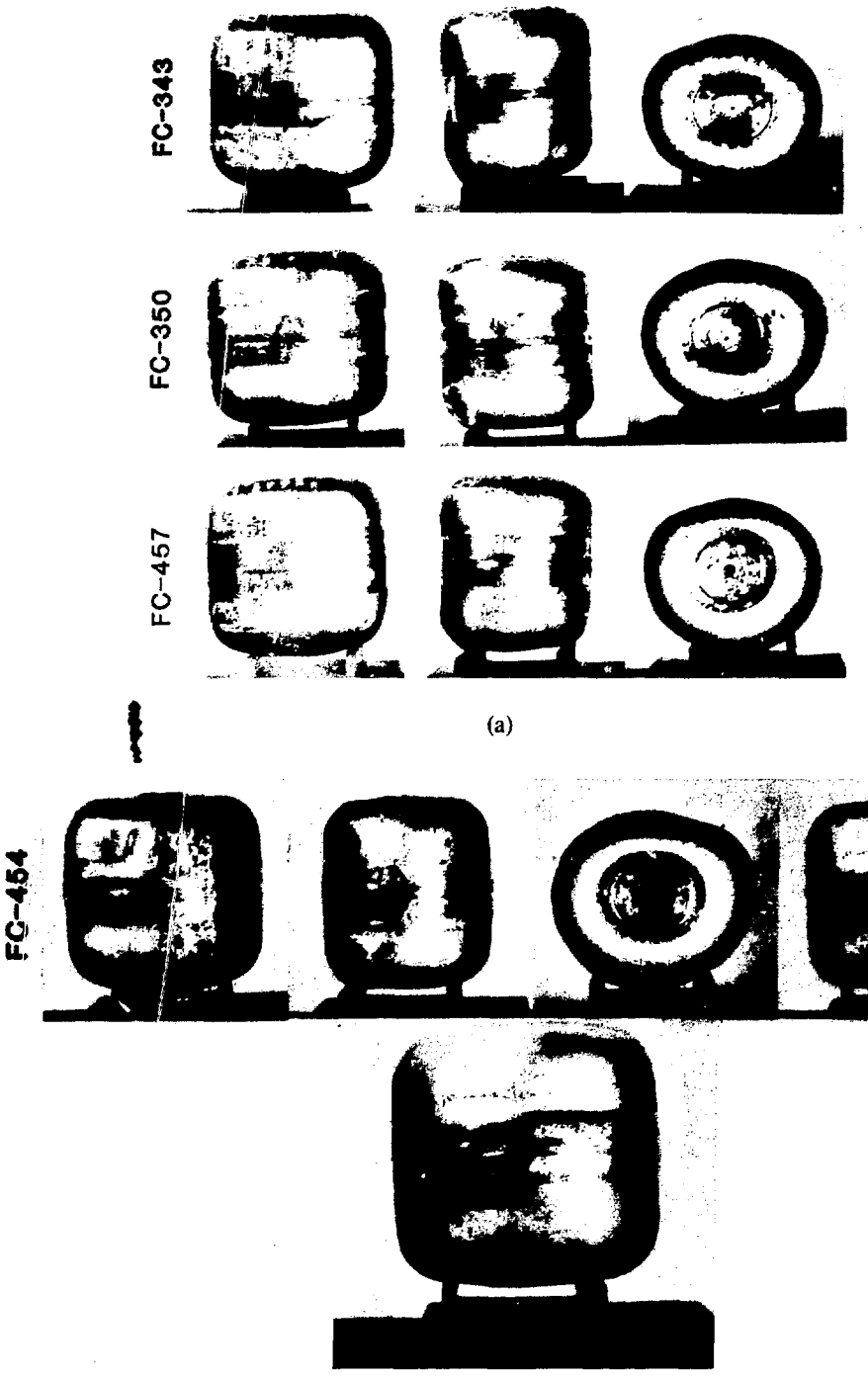

Fig. 4. Deformation of the impacted clads of test SVT-3: (a) fueled clads FC-343, -350, and -457 showing (l to r) impact face, side profile, and end profile (1X); (b) fueled clad FC-454 showing (*top*, l to r) impact face, side profile, end profile, and back side (1X) and (bottom) enlarged view of the back side with small crack in the shield cup (1.5X).

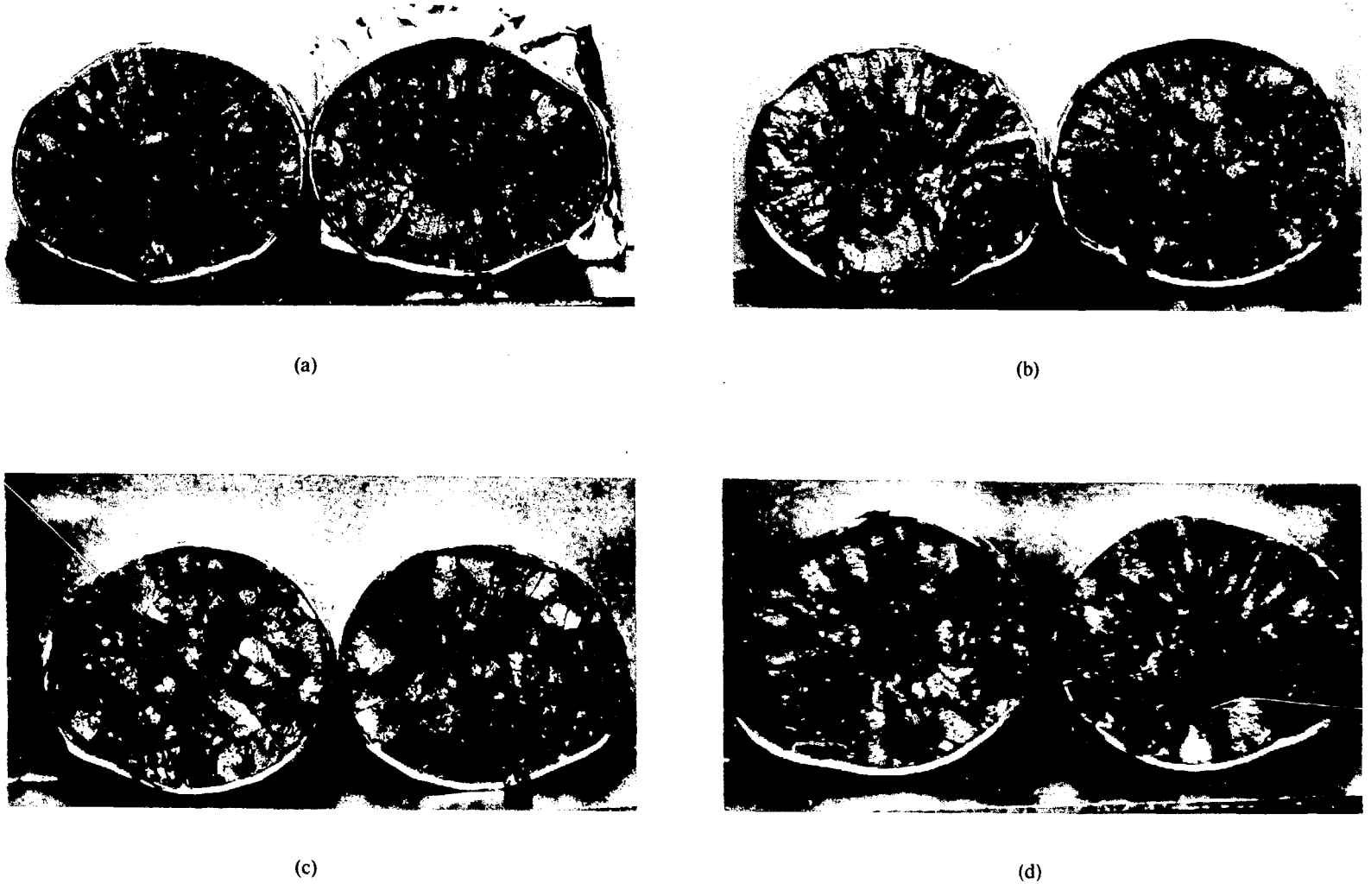

Fig. 5. Fracture patterns of the plutonia pellets of test SVT-3: (a) HF-343; (b) HF-350; (c) HF-454; (d) HF-457 (1.5X).

(a)

(b)

(c)

(d)

(e)

Fig. 6. Iridium microstructure of the shield cup of FC-454 (50X).

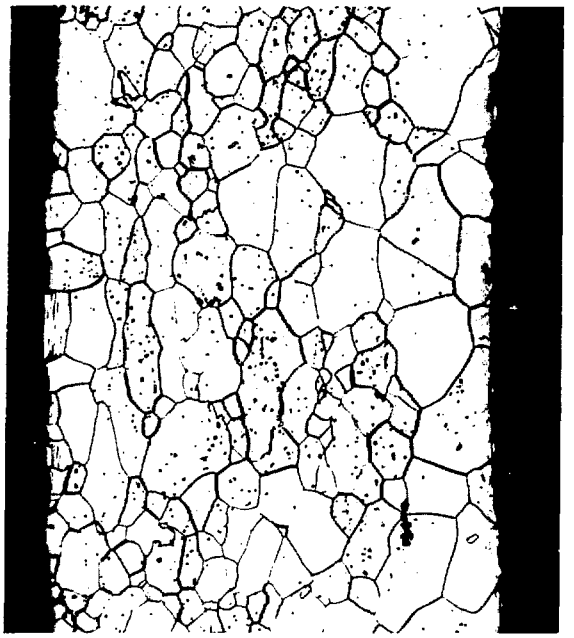

(a)

(b)

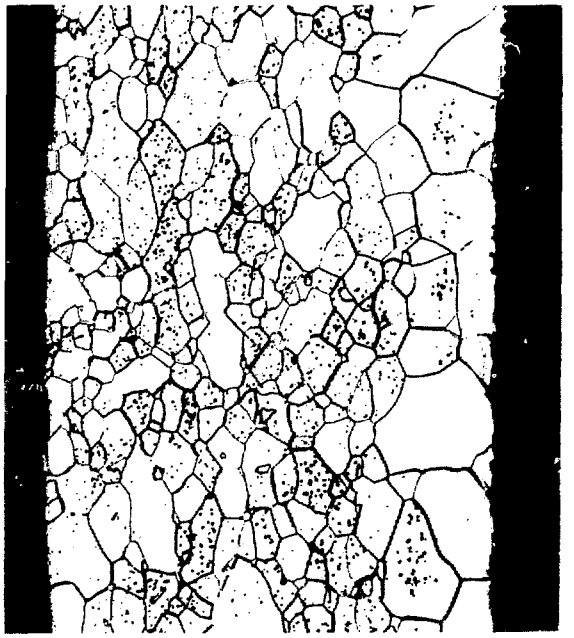

(c)

(d)

Fig. 7. Typical microstructures of the iridium of HF-343 and HF-350: (a) HF-343 vent cup; (b) HF-343 shield cup; (c) HF-350 vent cup; (d) HF-350 shield cup (100X).

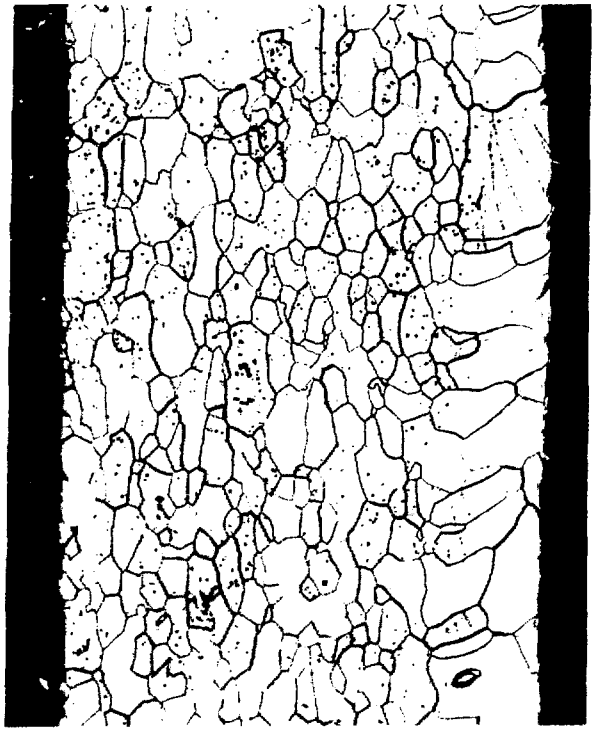

Fig. 8. Abnormal microstructure observed in transverse cross section of the shield cup of HF-350 (100X).

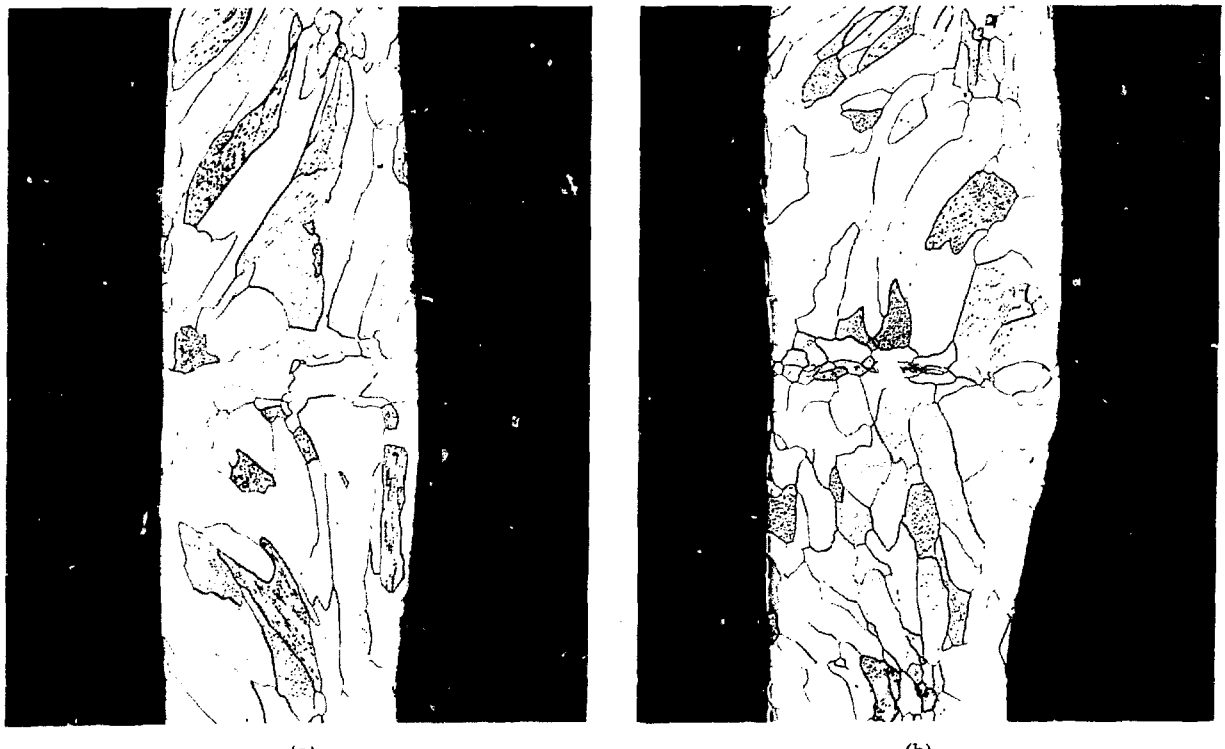

(a) (b)

Fig. 9. Microstructure of the weld bead of fueled clads of the prime impact assembly of test SVT-3: (a) HF-343; (b) HF-350 (50X).

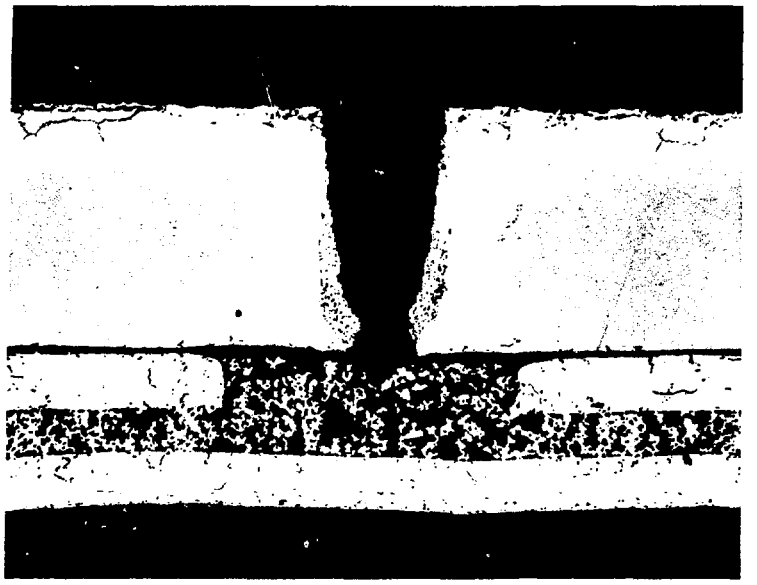

Fig. 10. As-polished cross section of the vent of HF-454 (50X).

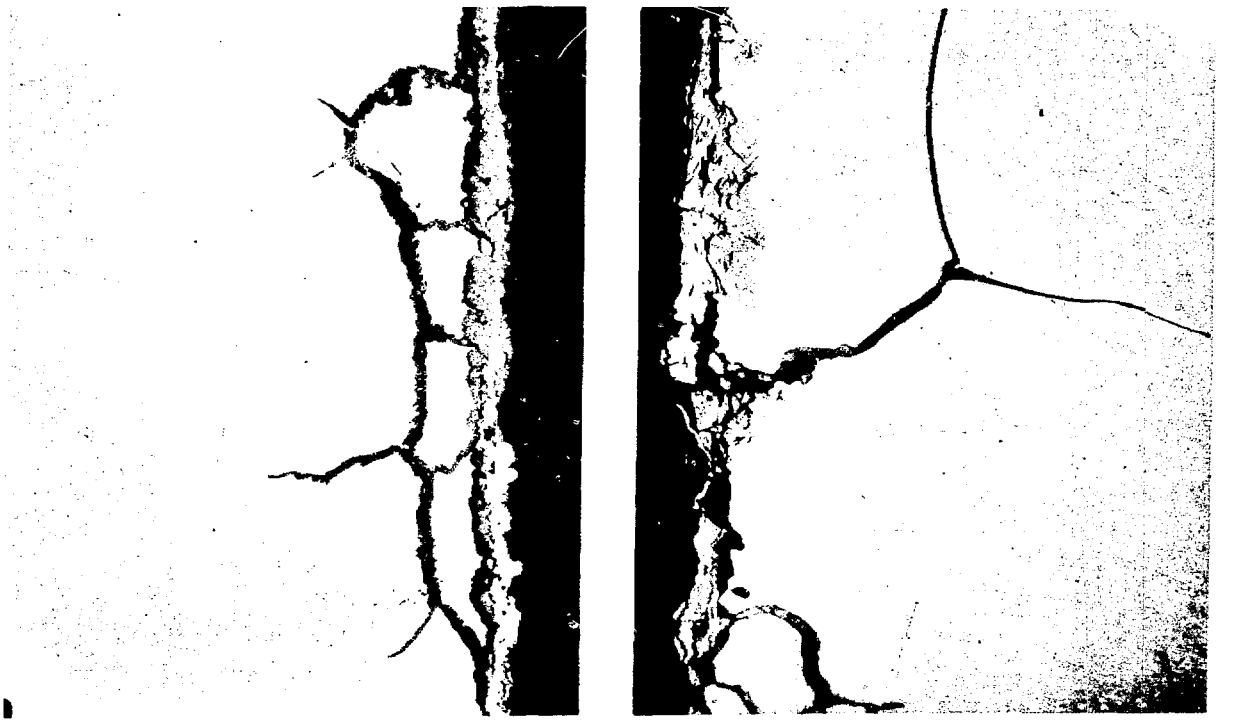

(a) (b)

Fig. 11. Intermetallic reaction products on the exterior of the clad of HF-454 (250X).

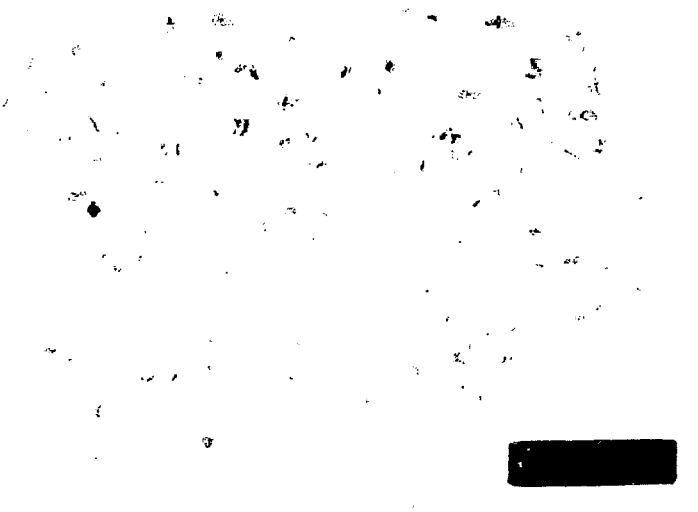

Fig. 12. The iridium fragments recovered after the DIRECT COURSE explosion were all small.

(a)

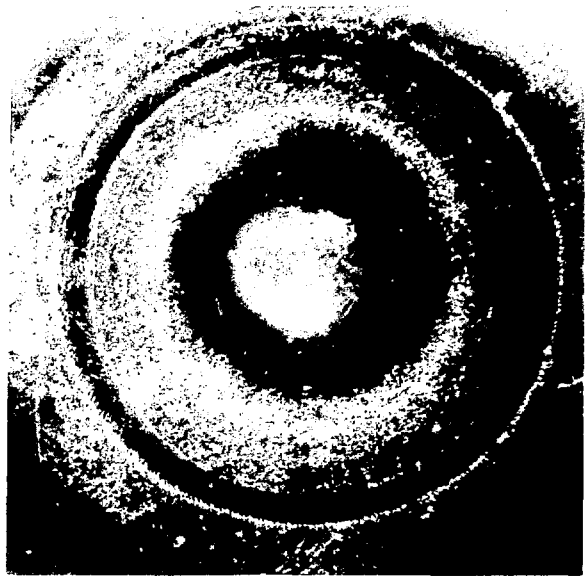

(b)

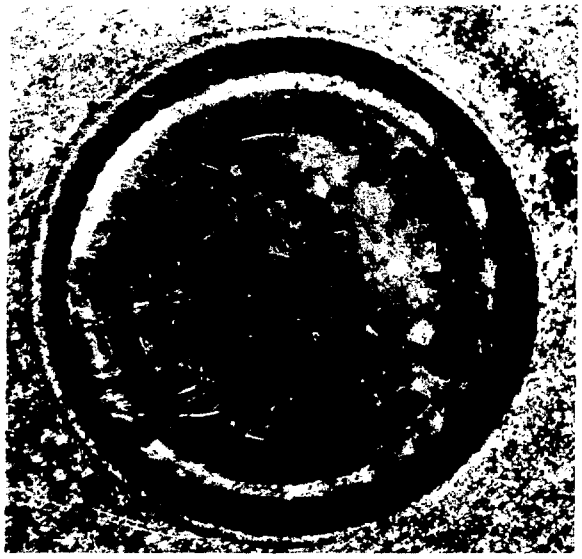

(c)

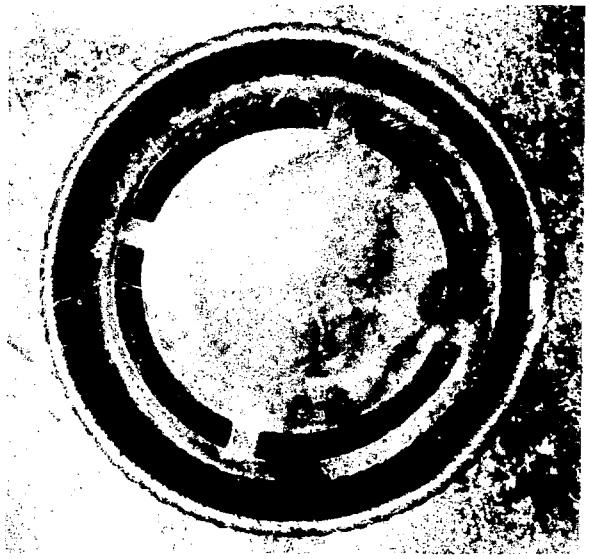

(d)

Fig. 13. There were cracks in the decontamination-cover welds of the two leaky capsules, but the interior structures were normal: (a) HF-104 with weld crack at 10 o'clock; (b) HF-219 with weld crack at 10 o'clock; (c) HF-104 interior vent structure; (d) HF-219 interior vent structure.(6:5X).

(a)

(b)

Fig. 14. The cracks in the leaky clads were near the inner circumferences of the decontamination-cover welds: (a) HF-104 (28X); (b) HF-219 (30X).

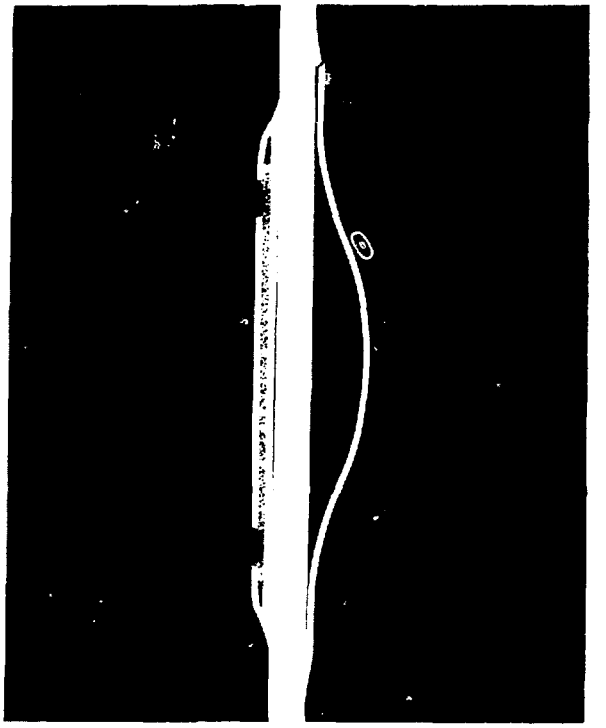

(a)

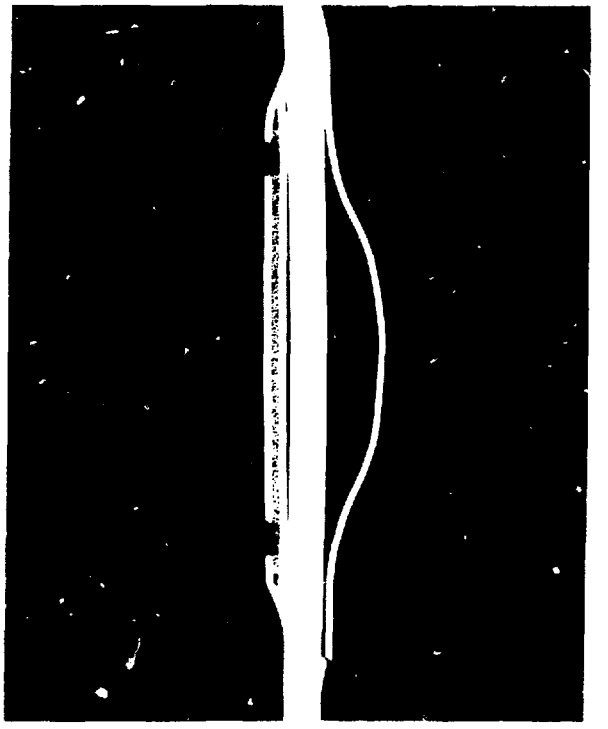

(b)

Fig. 15. The cracks penetrated both decontamination covers: (a) HF-104; (b) HF-219 (8X).

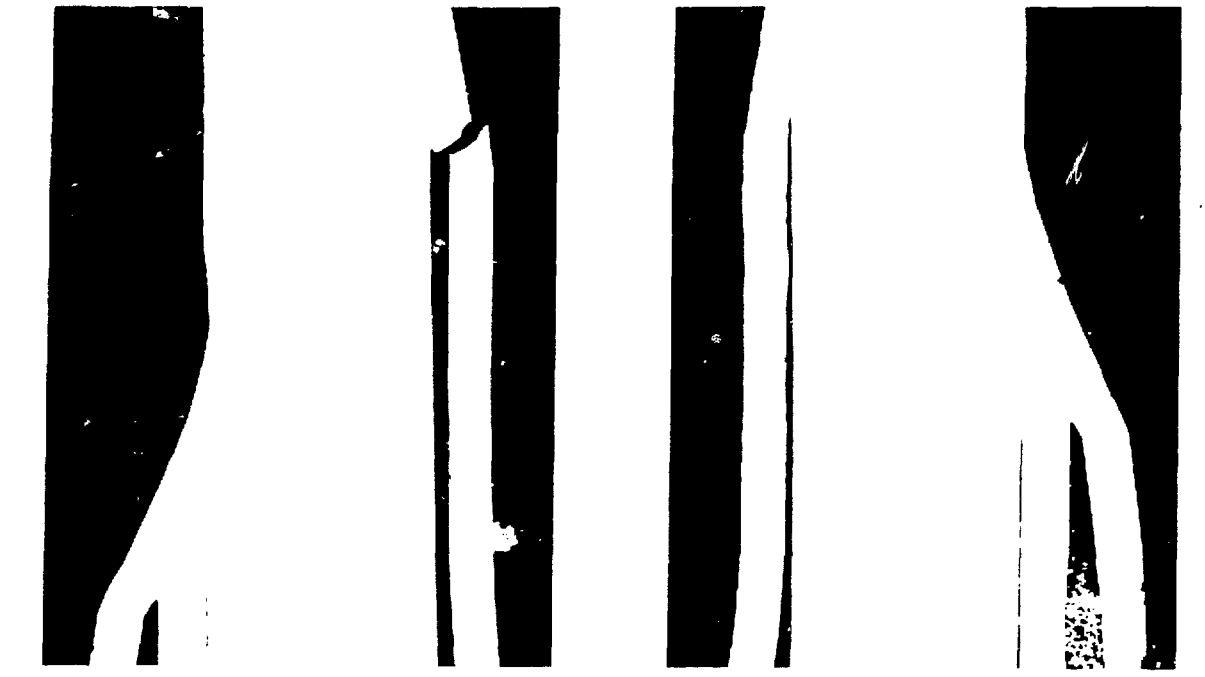

(a)

(b)

(c)

Fig. 16. All the cracks were close to the fillet of the decontamination-cover weld: (a) HF-104 breach; (b) HF-104 opposing crack; (c) HF-219 breach (50X).

Fig. 17. The cracks occurred in the columnar-grained weld metal: (a) HF-104; (b) HF-219 (50X).

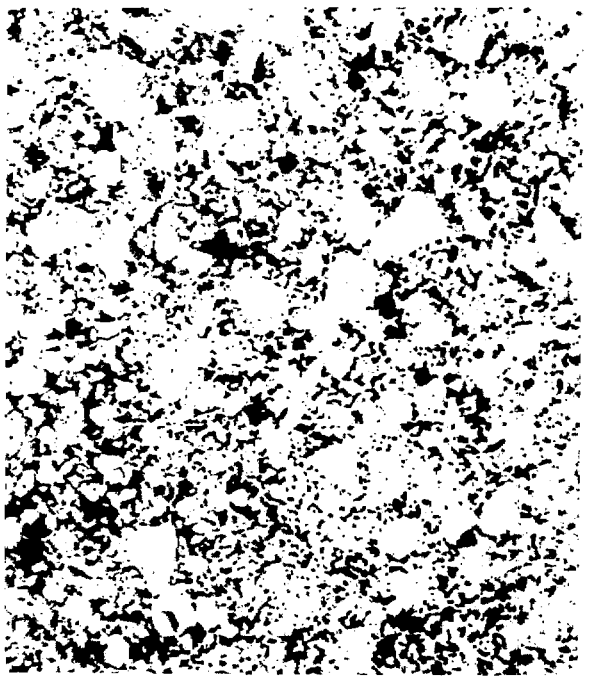

Fig. 18. Pellet ET 2-6 after 943 days in simulated seawater at 35°C, as polished (100X).

Fig. 19. Pellet ET 2-6 after 943 days in simulated seawater at 35°C, as polished (7X).

Fig. 20. Pellet ET 2-6 after 943 days in simulated seawater at 35°C, etched (100X).

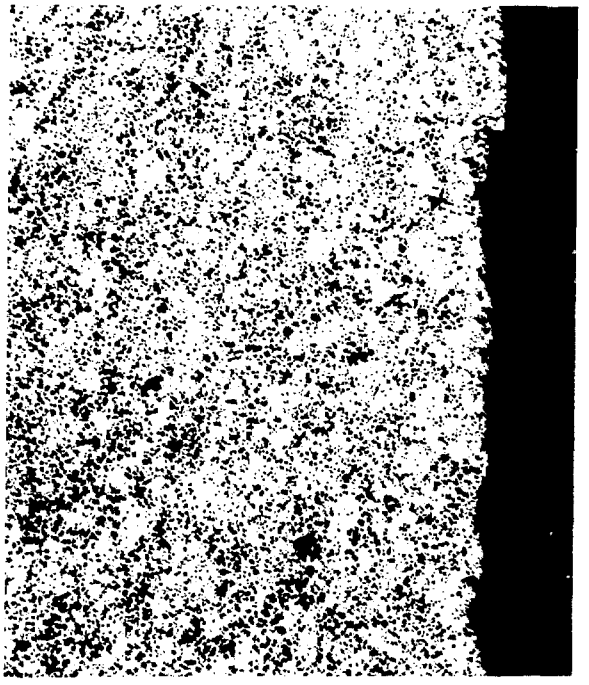

Fig. 21. Pellet ET 2-6 after 943 days in simulated seawater at 35°C, etched (50X).

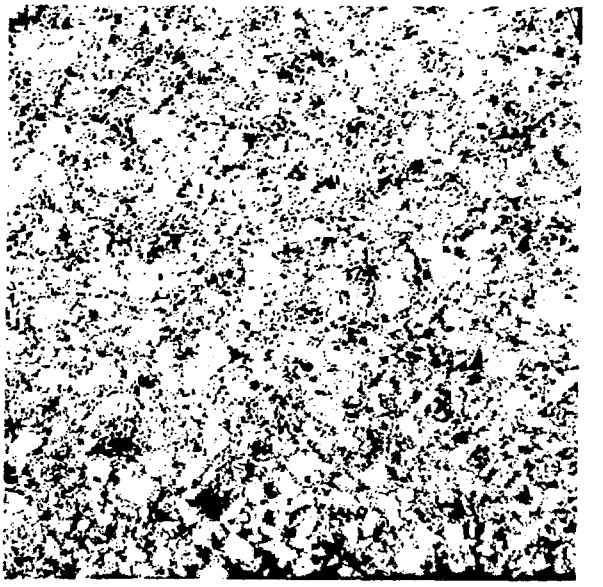

Fig. 22. Pellet ET 1-5 after 943 days in simulated seawater at 10°C, as polished (50X).

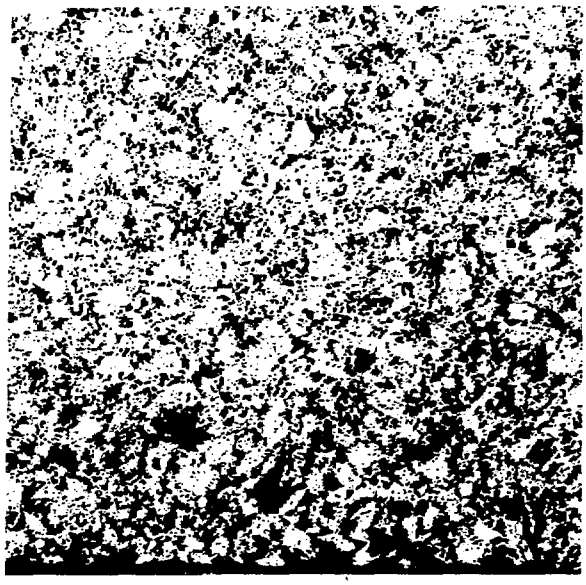

Fig. 23. Pellet ET 1-5 after 943 days in simulated seawater at 10°C, etched (50X).

Fig. 24. Pellet ET 1-5 after 943 days in simulated at 10°C, as polished (7X).

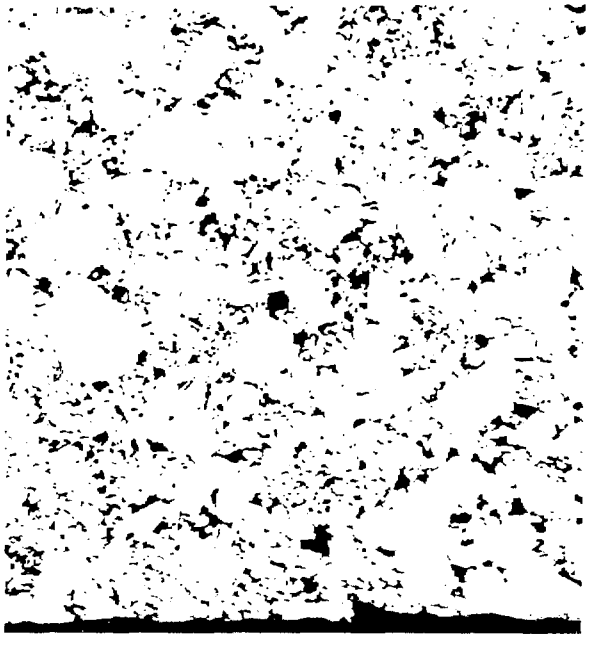

Fig. 25. Pellet HPZ-186-2 after 682 days in simulated seawater at 10°C, as polished (100X).

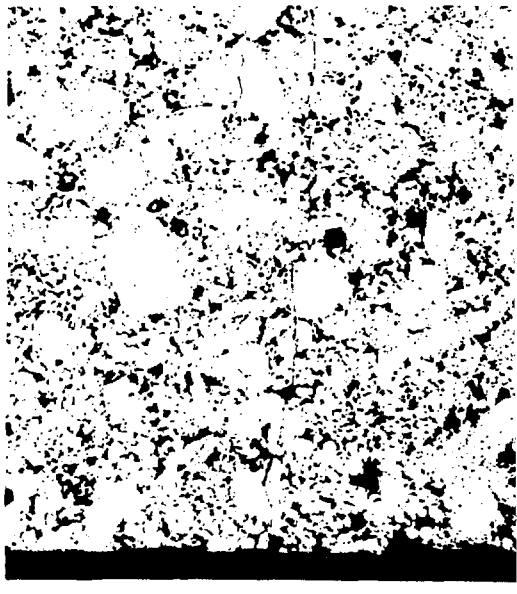

Fig. 26. A fragment from pellet HPZ-186-2 after 68 in simulated seawater at 10°C, etched (100X).

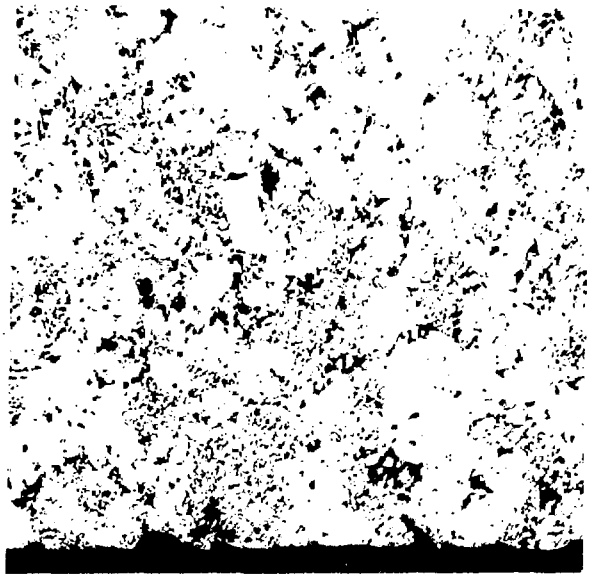

Fig. 27. Pellet HPZ-174-2 after 1855 days in simulated seawater at 10°C, as polished (100X).

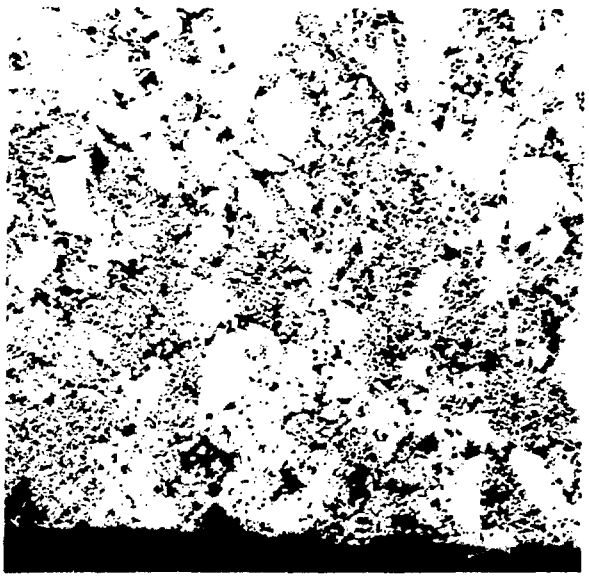

Fig. 28. Pellet HPZ-174-2 after 1855 days in simulated seawater at 10°C, etched (100X).

Fig. 29. Pellet ET 2-4 after 943 days in fresh water at 35°C, as polished (7X).

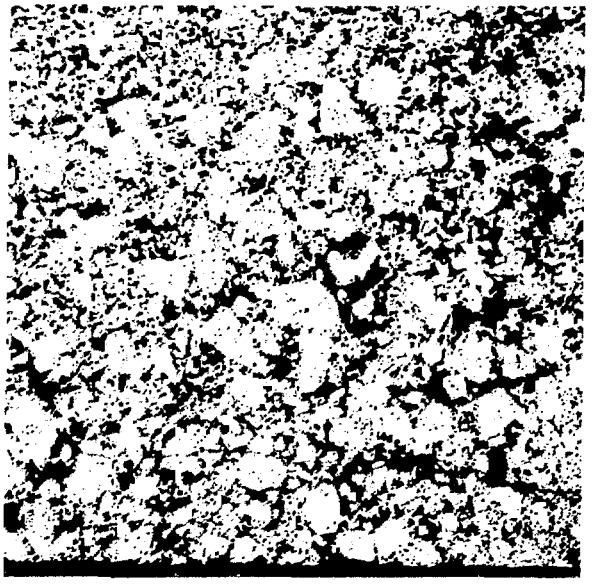

Fig. 30. Pellet ET 2-4 after 943 days in fresh water at 35°C, as polished (100X).

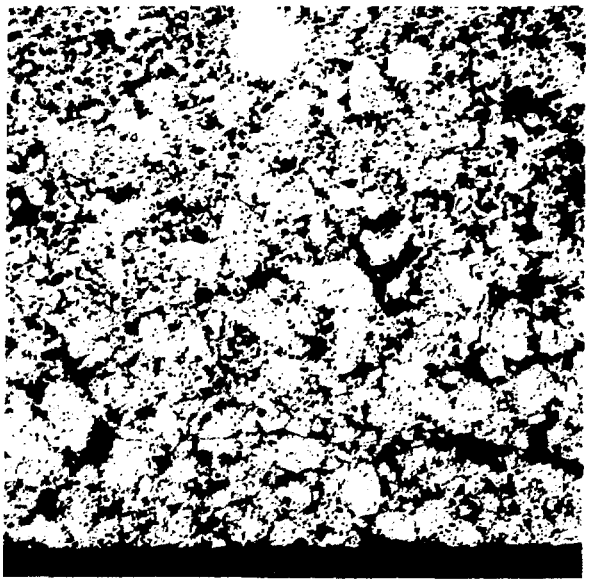

Fig. 31. Pellet ET 2-4 after 943 days in fresh water at 35°C, etched (100X).

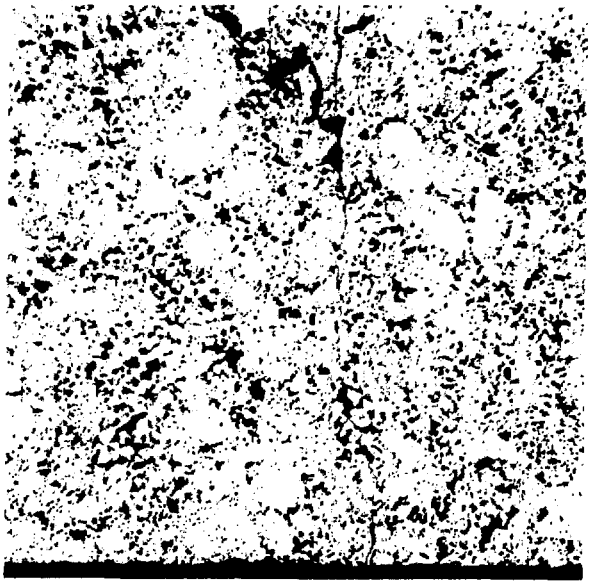

Fig. 32. Pellet ET 2-2 after 943 days in fresh water at 10°C, as polished (100X).

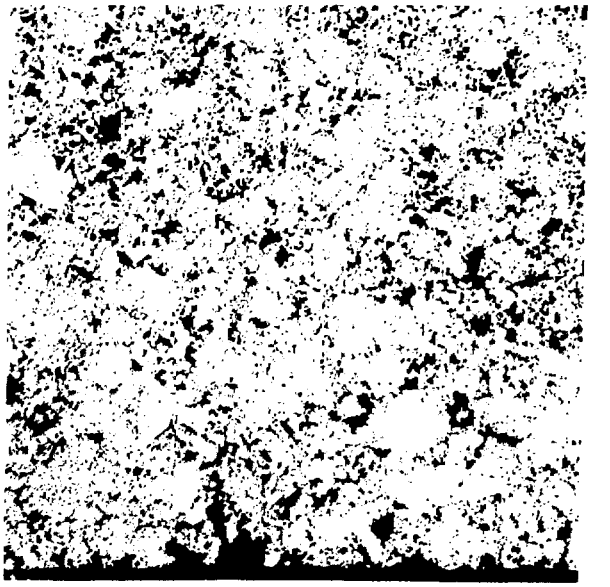

Fig. 33. Pellet ET 2-2 after 943 days in fresh water at 10°C, etched (100X).

Fig. 34. Impacted 5-W RTG heat source assembly (~1X).

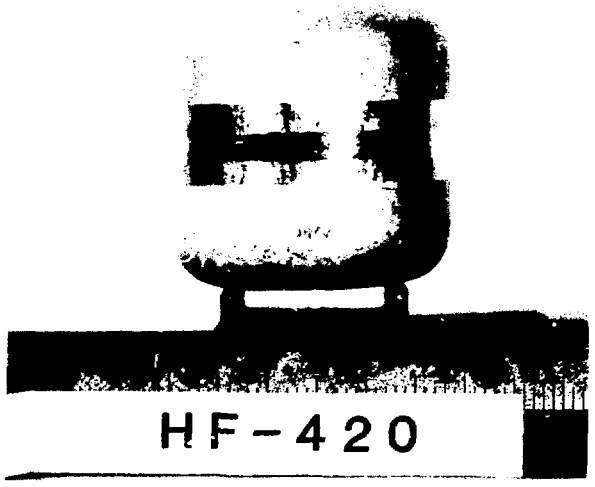

(a)

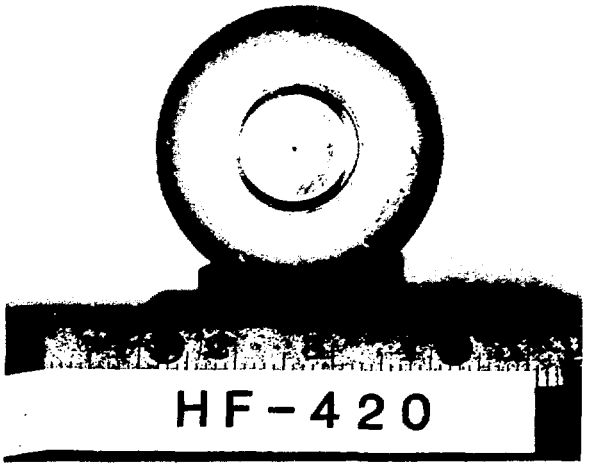

(b)

(c)

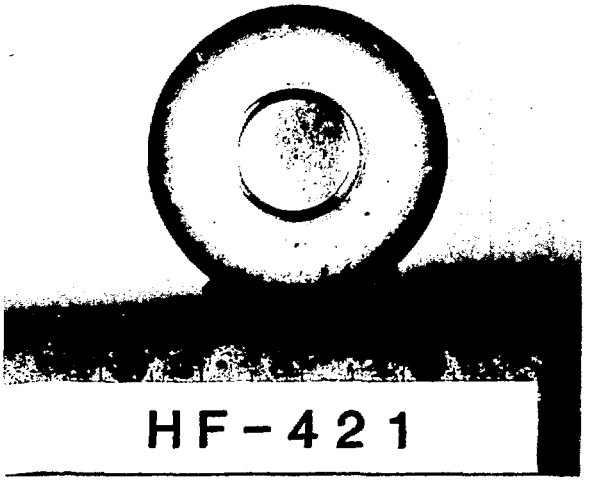

(d)

Fig. 35. Fueled clads of the 5-W RTG heat source after impact (~1.5X).

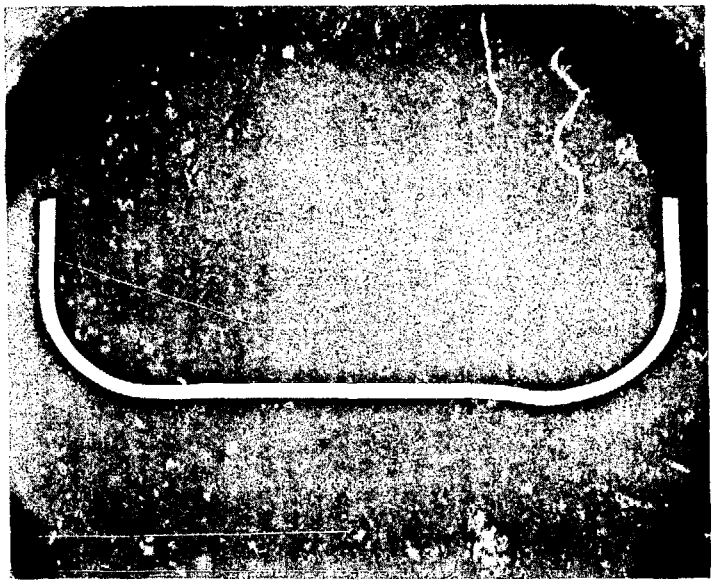

(a)

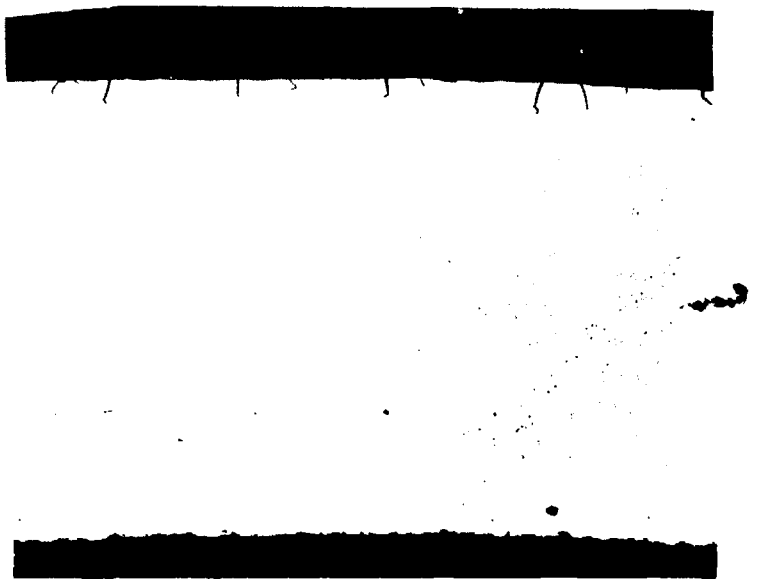

(b)

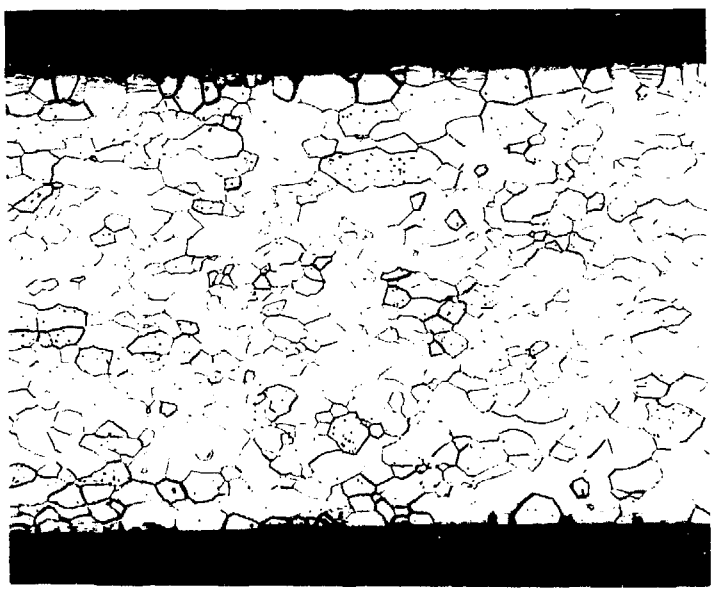

(c)

Fig. 36. Metallographic cross section of the impacted end of FC-421: (a) photomacrograph (3X); (b) as-polished photomicrograph (100X); (c) etched photomicrograph (100X).

ADDITIONAL DISTRIBUTION

B. J. Rock, Dept. of Energy/OSNP, Washington, DC
G. L. Bennett, Dept. of Energy/OSNP, Washington, DC
J. J. Lombardo, Dept. of Energy/OSNP, Washington, DC
J. Griffo, Dept. of Energy/OSNP, Washington, DC
D. K. Stevens, Dept. of Energy/BES, Washington, DC
M. Norin, Dept. of Energy, Washington, DC
N. P. Klug, Dept. of Energy, Washington, DC
L. Smith, Dept. of Energy, Washington, DC
E. Bjoro, Dept. of Energy, Washington, DC
G. H. Ogburn, Dept. of Energy, Washington, DC
C. Osterberg, Dept. of Energy, Washington, DC
I. Van Der Hoven, Dept. of Energy, Rockville, MD
J. V. Dorigan, Dept. of Energy Washington, DC
W. O. Forster, Dept. of Energy, Washington, DC
R. Watters, Dept. of Energy, Washington, DC
H. B. Rosenthal, Dept. of Energy, Washington, DC
Col. Terry Hawkins, ATSD (AE), Department of Defense, Washington, DC
Lt. Col. Jim Greening, HQ USAF/IG, Department of Defense, Washington, DC
D. L. Foster, Dept. of Energy, Albuquerque, NM
K. Elliot, Dept. of Energy, Albuquerque, NM
D. L. Krenz, Dept. of Energy, Albuquerque, NM
J. R. Roeder, Dept. of Energy, Albuquerque, NM
R. B. Crouch, Dept. of Energy, Albuquerque, NM
J. N. Bailey, Dept. of Energy, Albuquerque, NM
H. N Hill, Dept. of Energy/DOA, Miamisburg, OH
L. C. Sjostrom, Dept. of Energy, Aiken, SC
S. W. Ahrends, Dept. of Energy/ORO, Oak Ridge, TN
T. B. Kerr, NASA, Washington, DC
F. R. Schmidt, NASA, Washington, DC
Operations Space Shuttle, NASA, Washington, DC
A. V. Diaz, NASA, Washington, DC
R. G. Ivanoff, Jet Propulsion Laboratory, Pasadena, CA
R. W. Campbell, Jet Propulsion Laboratory, Pasadena, CA
L. C. Montgomery, Jet Propulsion Laboratory, Pasadena, CA
L. T. Shaw, Jet Propulsion Laboratory, Pasadena, CA
R. J. Spehalski, Jet Propulsion Laboratory, Pasadena, CA
Dr. Agnus D. McRonald, Jet Propulsion Laboratory, Pasadena, CA
P. Jaffe, Jet Propulsion Laboratory, Pasadena, CA
AFWL/NTYNS, Attn: Capt. D. E. Zimmerman, Kirtland AFB, NM
Lt. Col. James H. Lee, Jr., AFWL/NTYN, Kirtland AFB, NM
Capt. Michael K. Seaton, AFWL/NTYNP, Kirtland AFB, NM
Col. John Joyce, AFISC/SND, Kirtland AFB, NM
Maj. John Rice, AFISC/SNA, Kirtland AFB, NM
Maj. Ben Lucas, AFISC/SEM, Norton AFB, CA
Maj. James D. Martens, AFWL/NTX, Kirtland AFB, NM
Lt. Brett Haswell, AFWL/NTYNS, Kirtland AFB, NM
Capt. Nicholas Clemens, HW AFSC/IGF, Andrews AFB, MD
L. J. Ullian, ESMC/SEM, Patrick AFB, FL
Capt. John Leonowich, ESMC/SGPH, Patrick AFB, FL
Kenn Hill, ESMC/SEM, Patrick AFB, FL
Dr. W. Kessler, AFML/MPE, Wright-Patterson AFB, OH
Lt. Col. Dave Woods, AFISC/SGMS, Norton AFB, CA
John Marshall, AFRPL/LKHL, Edwards AFB, CA
Capt. Lance J. Bollinger, AFMSC/SGPZ, Brooks AFB, TX
Maj. John Burr, HQ AFMSC/SGPA, Brooks AFB, TX
W. Riley, WSMC/SEM, Vandenberg AFB, CA
Capt. Dennis Armstrong, USAF Hospital/SGPB, Vandenberg AFB, CA
Capt. James Lund, HQ SD/SE, Worldway Postal Center, Los Angeles, CA
Capt. Louis H. Schwichler, HQ SD/YOR, Worldway Postal Center, Los Angeles, CA
J. Mangino, SAMTO/DOD, Vandenberg AFB, CA
Maj. Frank P. Lahm, II, SAMTO/DOS, Vandenberg AFB, CA
W. T. Goldston, SRO, Aiken, SC
J. K. Brown, SRP, Aiken, SC
R. L. Folger, SRL, Aiken, SC
W. Amos, MRC, Miamisburg, OH
E. W. Johnson, MRC, Miamisburg, OH
W. B. Witmer, MRC, Miamisburg, OH
M. Martin, ORNL, Oak Ridge, TN
J. C. Hagan, APL, Laurel, MD
R. W. Jubach, NUS Corporation, Gaithersburg, MD
B. Bartram, NUS Corporation, Gaithersburg, MD
R. W. Englehart, NUS Corporation, Gaithersburg, MD
A. Schock, Fairchild-Hiller Ind., Germantown, MD
E. Skrabek, Fairchild-Hiller Ind., Germantown, MD
C. W. Whitmore, GE, Philadelphia, PA
C. T. Bradshaw, GE, Philadelphia, PA
J. Peterson, GE, Philadelphia, PA
R. Hemler, GE, Philadelphia, PA
V. Haley, GE, Philadelphia, PA
R. Hartman, GE, Philadelphia, PA
D. C. Anderson, Teledyne Energy Systems, Timonium, MD
P. Dick, Teledyne Energy Systems, Timonium, MD
M. Goldman, University of California, Davis, CA
C. Smith, Sandia National Laboratories, Albuquerque, NM
R. L. Hannigan, Sandia National Laboratories, Albuquerque, NM
C. M. Barnes, L. B. Johnson Space Center, NASA, Houston, TX
R. H. Brown, L. B. Johnson Space Center, NASA FM, Houston, TX
R. G. Rose, L. B. Johnson Space Center, NASA FA, Houston, TX
Harold Battaglia, L. B. Johnson Space Center, NASA PF, Houston, TX
W. H. Boggs, NASA, DE-A, J. F. Kennedy Space Center, FL
Lloyd Parker, NASA, SF, J. F. Kennedy Space Center, FL
George M. Marmaro, NASA, MD-ENV, J. F. Kennedy Space Center, FL
W. A. Riehl, Marshall Space Flight Center, NASA, EH31, Marshall SFC, AL
W. C. Pitts, NASA, STPM, Ames Research Center, Moffett Field, CA
J. J. Givens, Ames Research Center, Moffett Field, CA
Kenneth Sutton, Langley Research Center, NASA, Hampton, VA
Gerald D. Walberg, Langley Research Center, NASA, Hampton, VA
G. J. Schaefer, Jr., Lewis Research Center, NASA, LeRc-501, Cleveland, OH
D. Eaton, European Space Research and Technology Centre, Zwarteweg 62, Njordwijk, The Netherlands
Dr. Ralph R. Fullwood, Science Applications, Inc., Palo Alto, CA
D. Glenn, The Aerospace Corporation, Los Angeles, CA
Dr. William Ailor, The Aerospace Corporation, Los Angeles, CA
C. R. Chappell, Nuclear Regulatory Commission, Washington, DC
D. E. Janes, U. S. Environmental Protection Agency, Washington, DC
D. Eagan, Office of Radiation Programs, Washington, DC
James Boland, Argonne National Laboratory-West, Idaho Falls, ID
N. Elsner, General Atomics, San Diego, CA
R. F. Abbey, Naval Research Laboratory, Washington, DC
Charles Salisbury, Naval Ocean Systems Center, San Diego, CA
Dr. Herbert Weiss, Naval Ocean Systems Center, San Diego, CA
R. Cuddihy, IIT Research Institute, Chicago, IL
J. F. Park, Pacific Northwest Laboratory, Richland, WA
Thomas M. Beasley, Oregon State University, Newport, OR
Jackson O. Blanton, Skidaway Inst. of Oceanography, Savannah, GA
Martha Scott, Texas A&M University, College Station, TX
H. James Simpson, Columbia University, Palisades, NY

R. N. R. Mulford, Los Alamos National Laboratory, Los Alamos, NM
J. Birely, Los Alamos National Laboratory, Los Alamos, NM
S. E. Bronisz, Los Alamos National Laboratory, Los Alamos, NM
G. Rinehart, Los Alamos National Laboratory, Los Alamos, NM
R. W. Zocher, Los Alamos National Laboratory, Los Alamos, NM
J. A. Pattillo, Los Alamos National Laboratory, Los Alamos, NM
E. M. Wewerka, Los Alamos National Laboratory, Los Alamos, NM
T. C. Wallace, Los Alamos National Laboratory, Los Alamos, NM
J. Boudreau, Los Alamos National Laboratory, Los Alamos, NM
C. M. Seabourn, Los Alamos National Laboratory, Los Alamos, NM
P. Wagner, Los Alamos National Laboratory, Los Alamos, NM